Nearest-neighbor connectedness theory: A general approach to continuum percolation

Fabian Coupette,[1] René de Bruijn,[2,*] Petrus Bult,[2] Shari Finner,[2] Mark A. Miller,[3] Paul van der Schoot,[2] and Tanja Schilling[1,†]

[1]*Institute of Physics, University of Freiburg, Hermann-Herder-Straße 3, 79104 Freiburg, Germany*

[2]*Department of Applied Physics, Eindhoven University of Technology, P.O. Box 513, 3500 MB Eindhoven, The Netherlands*

[3]*Department of Chemistry, Durham University, South Road, Durham DH1 3LE, United Kingdom*

(Received 17 December 2020; accepted 19 March 2021; published 8 April 2021)

We introduce a method to estimate continuum percolation thresholds and illustrate its usefulness by investigating geometric percolation of noninteracting line segments and disks in two spatial dimensions. These examples serve as models for electrical percolation of elongated and flat nanofillers in thin film composites. While the standard contact volume argument and extensions thereof in connectedness percolation theory yield accurate predictions for slender nanofillers in three dimensions, they fail to do so in two dimensions, making our test a stringent one. In fact, neither a systematic order-by-order correction to the standard argument nor invoking the connectedness version of the Percus-Yevick approximation yield significant improvements for either type of particle. Making use of simple geometric considerations, our new method predicts a percolation threshold of $\rho_c l^2 \approx 5.83$ for segments of length l, which is close to the $\rho_c l^2 \approx 5.64$ found in Monte Carlo simulations. For disks of area a we find $\rho_c a \approx 1.00$, close to the Monte Carlo result of $\rho_c a \approx 1.13$. We discuss the shortcomings of the conventional approaches and explain how usage of the nearest-neighbor distribution in our method bypasses those complications.

DOI: 10.1103/PhysRevE.103.042115

I. INTRODUCTION

The electrical, thermal, and mechanical properties of polymeric materials can be controlled by the addition of (conductive) nanofillers, producing what may be called functional nanomaterials. For fillers to strongly affect the properties of the polymeric host material, a material-spanning network of connected particles is required. Here, connectivity is defined in terms of a length scale below which the particles are able to effectively exchange charge carriers, heat, or other quantities to be transported. The formation of such a network is a geometrical transition akin to a phase transition, and the set of conditions for which this occurs is referred to as the percolation threshold. Commonly used fillers are, for instance, metallic nanowires and carbon nanotubes [1,2], whose highly elongated shape is known to be ideal for producing the required material spanning network at very low filler fractions [3].

A wide range of possible application areas is currently under investigation, including mechanical stress sensing, actuation, energy harvesting, electromagnetic interference shielding, and optoelectronics in the form of transparent thin film electrodes [4–10]. In many of these application areas, it is crucial for the material to have barely crossed over from an insulating to a conductive state, either in order to keep the particle loading as low as possible or to maximize the response to an external stimulus. It stands to reason that a deeper theoretical understanding of the percolation threshold should be conducive to a rational design of novel composite materials.

Our theoretical understanding of percolation of slender nanofillers in three-dimensional bulk materials has improved significantly over the past decades since the pioneering works of Bug *et al.* [11] and of Balberg *et al.* [3], in particular for particles that interact via a harshly repulsive excluded volume [12]. This is not the case for percolation of slender particles in quasi-two-dimensional materials, that is, composite films of which the height is much smaller than the length of the filler particles [13,14]. These quasi-two-dimensional materials are often modeled as two-dimensional systems, consisting of noninteracting fillers that are defined to be connected if they overlap.

Even for such an ideal model system, applying the common contact volume argument to pinpoint the percolation threshold is highly inaccurate in two dimensions, despite it being asymptotically exact for infinitely slender fillers in three dimensions. As the contact volume argument neglects direct connections between more than two neighboring particles, this approximation is similar in spirit to that of the Onsager theory for the isotropic-to-nematic phase transition of hard rodlike particles, which fails to accurately describe the same phase transition in two dimensions [15,16].

In this article we show that neither a systematic expansion in increasing powers of the density nor the connectedness version of Percus-Yevick (cPY) approximation significantly improve predictions obtained within the second virial approximation. To remedy this, we propose a method that is conceptually simple, yet has a significantly improved accuracy in predicting the percolation threshold, in particular for systems in which the percolating cluster contains large loops

*r.a.j.d.bruijn@tue.nl

†tanja.schilling@physik.uni-freiburg.de

of connected particles. As the method is similar to connectedness percolation theory (CPT) but uses the nearest-neighbor distribution as input, we dub it nearest-neighbor connectedness percolation theory (NNCPT).

NNCPT uses neither a density expansion nor a closure relation taken from liquid state theory. Instead, closure is obtained by geometrical arguments regarding the cluster structure at short distances, while the behavior at long distances is obtained by a renormalization-group-type argument. The method is exact for one-dimensional systems and reproduces the correct low density limit in higher dimensions. The computation of the percolation threshold is numerically simple, and the framework can easily be applied to arbitrary pair interactions if the corresponding nearest-neighbor distribution is inserted. Thus, our method provides a reliable way to estimate percolation thresholds for systems where conventional approaches are known to struggle—two-dimensional ideal particles forming excellent benchmark systems. In the remainder of this paper, we first apply connectedness percolation theory to ideal line segments and disks testing a virial expansion and the Percus-Yevick closure. Then we introduce nearest neighbor connectedness theory and apply it to ideal line segments and disks.

II. CONNECTEDNESS PERCOLATION THEORY

Given the success of CPT in predicting percolation thresholds of a large class of three-dimensional systems, we begin by recalling its basic notions and then apply them to the two-dimensional case: The pair connectedness function $P(1,2)$ is defined such that $\rho(1)\rho(2)P(1,2)d1d2$ is the probability that particle 1 and particle 2 are part of a cluster of connected particles [17]. Here, $\rho(1)$ and $\rho(2)$ are single-particle number densities, the labels 1 and 2 represent the degrees of freedom of the particles (including orientations), and $d1, d2$ are the corresponding phase space volumes [18]. For $P(1,2)$, a connectedness equivalent to the Ornstein-Zernike (cOZ) equation can be obtained:

$$P(1,2) = C^{+}(1,2) + \int d3\, \rho(3) C^{+}(1,3) P(3,2), \quad (1)$$

where $C^{+}(1,2)$ is the so-called direct connectedness function. The mean cluster size S is given by

$$S = 1 + \lim_{q\to 0} \rho \langle \widehat{P}(q, \vartheta_{12}) \rangle = \lim_{q\to 0} (1 - \rho \langle \widehat{C}^{+}(q, \vartheta_{12}) \rangle)^{-1}, \quad (2)$$

where ρ is the average particle number density, the hat indicates a Fourier transform, q denotes the magnitude of the wave vector, ϑ_{12} is the relative orientation between the particles, and the brackets $\langle \cdots \rangle$ describe the angular average over the orientations of both particles. The final expression applies only for translationally and rotationally invariant distributions but is independent of particle shape [19]. The percolation threshold is given by the density ρ_c for which S diverges.

Hence, we only require $C^{+}(1,2)$ to calculate the percolation threshold. This direct connectedness function is, however, typically not known in closed form. The simplest method to approximate it is to make use of a series expansion in the density, similar to the virial expansion describing thermodynamic properties of dispersions [17]

$$\lim_{q\to 0} \widehat{C}^{+}(q) = \sum_{n=0}^{\infty} \rho^n C^{+}_{n+2}. \quad (3)$$

To describe percolation of three-dimensional slender particles, the expansion of Eq. (3) can be truncated after the C_2^{+} term. This truncation, known as the second virial approximation of connectedness percolation theory, corresponds to the assumption that the cluster has a treelike structure, and, as it yields mean-field critical exponents, can be considered a mean-field approximation in percolation theory. While believed to be asymptotically exact for infinitely slender particles in three dimensions [11], its prediction for two-dimensional line segments is far less accurate. Using the analytical expression $C_2^{+} = 2l^2/\pi$ for line segments of length l yields $\rho_c l^2 = \pi/2$, which deviates by a factor of 3.6 from Monte Carlo simulation results [20]. The situation is even worse for disks, where the disparity is a factor of 4.5 (see Table I). To improve upon this unsatisfactory situation one could, perhaps naively, either extend the estimate of C^{+} in an order-by-order fashion, or make use of the extensive toolbox of closures obtained from liquid-state theory [17,21].

TABLE I. Percolation threshold ρ_c obtained from Monte Carlo simulations [20], the method NNCPT, the virial expansion up to fourth order, the connectedness Percus-Yevick theory [23], and a Padé approximant [24] in the mean cluster size for overlapping lines of length l and disks of area a.

Method	Line segments ($\rho_c l^2$)	disks ($\rho_c a$)
Monte Carlo	5.6372858(6)	1.12808737(6)
NNCPT	5.83	1.00
Second virial	$\pi/2 \approx 1.57$	$\frac{1}{4}$
Third virial		
Fourth virial	24.0 ($\sigma = 0.1$)	0.326838...
cPY		
[2,1]-Padé approximant	3.878 ($\sigma = 10^{-3}$)	0.748742...

For the order-by-order approach, we use the known analytical expression for the third hard-body virial coefficient B_3 for line segments [22], which can be linked to C_3^{+} by $C_3^{+} = -3B_3$. Truncating after C_3^{+} produces two imaginary and hence unphysical predictions for the percolation threshold. Higher order terms can be obtained by Monte Carlo integration. Truncating after $C_4^{+} l^{-6} = (0.00548 \pm 0.00002)$ we obtain two imaginary roots and one real root, $\rho_c l^2 = 24.0 \pm 0.1$. Hence, going up to fourth order does not provide any improvement upon the second virial approximation. Moreover, the mean cluster size S obtained within the third and the fourth virial approximation produces a nonmonotonic function of the scaled density (see Fig. 1). S even becomes smaller than unity, indicating negative connectivity probabilities and highlighting the problems with the virial expansion. The same happens for overlapping disks (see Table I).

Rather than adding virials, we next invoke the cPY closure [25]. If expressed in terms of a diagrammatic expansion of the pair connectedness function, all diagrams representing the second and third virials are contained exactly, but higher order ones are incomplete [26,27]. For the thermodynamic

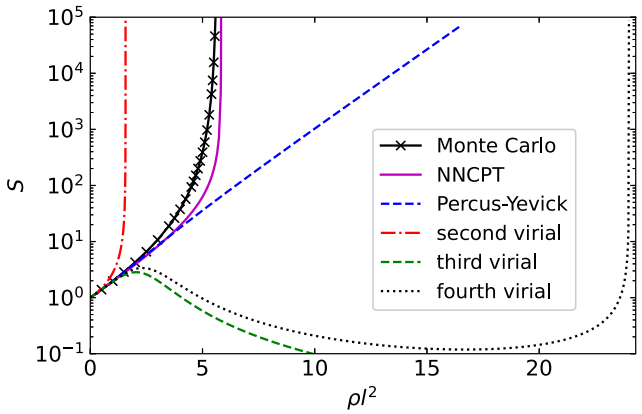

FIG. 1. Mean cluster size of overlapping line segments in two dimensions. The third and fourth virial approximations give non-monotonic curves, and the cPY prediction does not diverge for densities below $\rho l^2 = 17$.

properties of hard particles, these diagrams turn out to be unimportant. However, as we shall see, they are important in the context of percolation in systems in which the percolating cluster contains large loops.

The cPY closure needs to be solved self-consistently in conjunction with the cOZ equation. We tackle this numerically using a rotational invariant expansion (see Supplemental Material [28]). We iterate the governing set of equations by a modified Picard iteration [29,30] for all densities up to the one where the iterations no longer converge and percolation is achieved. As shown in Fig. 1, there is neither a percolation threshold for line segments nor for disks [23].

Hence we suggest that methods borrowed directly from liquid state theory must be inherently inaccurate when applied to percolation problems. We attribute the failure of these methods to ignoring loop correlations involving very large numbers of particles. To test for the occurrence of such loops, we carried out a simulation, in which we dropped line segments on the plane randomly with positions and orientations drawn uniformly. We then identified all clusters of intersecting line segments and counted the loops in the backbone of each cluster. In Fig. 2 we show a snapshot at a density just below

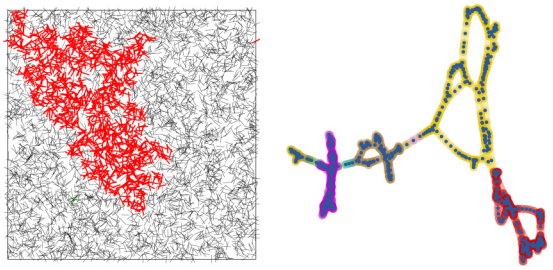

FIG. 2. Left: Simulation snapshot at $\rho l^2 = 5.0$; the largest connected cluster is marked in red. Right: Backbone of the network connecting two rods within the largest cluster. Colors correspond to different non-nodal components. Some of these contain large loops, hence a virial expansion of the direct connectedness function is expected to fail.

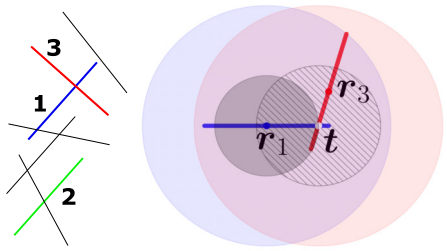

FIG. 3. Left: Construction of the pair connectedness function in NNCPT. Right: Effective treatment of the union of a segment and its nearest neighbor as weighted disks: the hatched disk represents the nearest neighbor; the large transparent disks form the *surface* $A_{1\cup3}$ with the exception of the dark disk, which is blocked by the nearest-neighbor condition.

the percolation transition. On the right we show the structure of the backbone of the largest cluster. The various non-nodal components (i.e., sections where no single particle lies on all paths between the end points) are colored differently. Large loops consist of many particles, and can therefore not be captured by a low order expansion, as the nth coefficient C_n^+ in the truncated virial expansion describes loops consisting of at most n particles. This suggests that a different theoretical approach is needed altogether that we suggest next.

III. NEAREST-NEIGHBOR CONNECTEDNESS PERCOLATION THEORY

In contrast to the work by Coniglio *et al.* [17], we construct the pair connectedness function $P(1,2)$ iteratively by going from particle 1 to its nearest neighbor (particle 3 in Fig. 3). If particle 1 is not connected to its nearest neighbor, it cannot be part of any connected cluster. If it is connected, we treat the union of both particles as a "new particle 1" and repeat the process until we reach particle 2. Thus $P(1,2)$ can be written as

$$P(1,2) = f^+(1,2)+[1-f^+(1,2)]\int d3\omega^+(1,3)P(3,2|3n1). \tag{4}$$

Here, f^+ denotes the probability that particles 1 and 2 are directly connected. ω^+ is the probability density to encounter the nearest neighbor of 1 in the phase space volume $d3$, while also being connected to it. (ω^+ differs from f^+, as f^+ refers to any connection, while ω^+ only refers to the connection with the nearest neighbor. Both functions need to be defined suitably for a given particle geometry) $P(3,2|3n1)$ is the conditional probability that 3 and 2 are part of the same cluster, given that 3 is the nearest neighbor of 1.

Compared to Eq. (1), Eq. (4) bears the disadvantage that it connects two different types of probability. We hence define the ratio

$$c(3,2|3n1) := \frac{P(3,2|3n1)}{P(3,2)}$$

and obtain our alternative to the cOZ equation, the nearest-neighbor connectedness equation

$$P(1,2) = f^+(1,2) + [1 - f^+(1,2)] \times \int d3\, \omega^+(1,3) c(3,2|3n1) P(3,2). \quad (5)$$

Here, f^+ is a known function, which depends on the specific geometry of the problem, while P, ω^+, and c are in general not known. However, in contrast to the direct connectedness function in Eq. (1), which involves an infinite sum of arbitrarily complicated diagrams, the nearest-neighbor distribution ω^+ can be approximated or even determined exactly using thermodynamic correlation functions, and a closure for Eq. (5) can be obtained c based on geometric considerations. Moreover, if we assume c to be independent of particle 2, Eq. (5) is reduced to a convolution. Close to percolation this is a reasonable assumption, because irrespective of the distance between particle 2 and particle 3, what matters for $P(3,2)$ is whether they are part of the percolating cluster. For one-dimensional systems this statement is actually exact [31]. Once the problem is simplified in this way, the remaining task is to find the density at which the integral over the complete integral kernel exceeds one.

IV. RESULTS AND DISCUSSION

We now apply NNCPT to freely penetrable line segments. The relative position of two segments with respect to each other is given by their orientations and their center-to-center distance $\boldsymbol{r}_{12}$. The connectivity criterion, which determines whether two segments intersect each other, is invariant under rotations of the whole system. Thus, in place of two orientational degrees of freedom, we only need to account for the relative orientation ϑ_{12}. Using translational invariance of the connectivity criterion, we are free to choose segment 1 as centered in the origin parallel to the x axis. We need to specify f^+, ω^+, and c. $f^+(\boldsymbol{r}_{12}, \vartheta_{12})$ is 1 if the segments intersect each other and zero if they do not. To specify ω^+, we define as the nearest neighbor the segment which intersects segment 1 closest to its center. ω^+ can be expressed as a function of the intersection point $\boldsymbol{t}$ along segment 1. Note that if a segment intersects at a point $\boldsymbol{t}$, the center position of the nearest neighbor completely defines its orientation. The center of a segment 3, $\boldsymbol{r}_3$, which intersects segment 1 at position $\boldsymbol{t}$, can be anywhere within a circle of diameter l around $\boldsymbol{t}$ with uniform probability. As a consequence, the nearest-neighbor distribution becomes an exponential evenly distributed on a disk:

$$\omega^+(\boldsymbol{r}_3, t) = \frac{4}{\pi l^2} \Theta\left(\frac{l}{2} - |\boldsymbol{r}_3 - \boldsymbol{t}|\right) \frac{2}{\pi} \rho l \exp\left(-\frac{4\rho l}{\pi}|t|\right), \quad (6)$$

with the number density of segments ρ, t the projection of $\boldsymbol{t}$ on the x axis, and Θ the Heaviside function. Notice that we fixed the orientation of segment 1 so that ω^+ depends only on t and not on $\boldsymbol{t}$.

The last function to specify is c, which measures how much the probability of a connection between segments 3 and 2 is influenced by the existence of segment 1. This probability is the result of two competing effects. On the one hand, two segments together offer more phase space than a single one for other segments to connect to. On the other hand, a portion of this phase space is blocked by the condition that 3 is the nearest neighbor of 1. We argue that close to the percolation threshold, the only relevant difference between a single segment and two intersecting segments is their *surface* in phase space. If we choose c as a function of the surface in phase space, it apparently does not depend on segment 2 anymore—our first approximation—but still on the detailed microscopic arrangement of segments 1 and 3. Equation (5) thus reads

$$P(\boldsymbol{r}_{12}, \vartheta_{12}) = f^+(\boldsymbol{r}_{12}, \vartheta_{12}) + [1 - f^+(\boldsymbol{r}_{12}, \vartheta_{12})] \times \int_{-l/2}^{l/2} dt \int d\boldsymbol{r}_3 \omega^+(\boldsymbol{r}_3, t) c(\boldsymbol{r}_3, t) P(\boldsymbol{r}_{32}, \vartheta_{32}). \quad (7)$$

Finally, we eliminate the angular dependencies. We interpret each line segment as a weighted disk, i.e., smeared out over all possible orientations. The contact function $f^+(1,2)$ becomes the overlap of two disks with center separation r_{12} reproducing the correct angular average $f^+(r_{12}) := \langle f^+(1,2)\rangle_{\vartheta(r_{12})}$. In order to construct c, we consider the combination of two disks as a single disk with a new diameter that offers the same phase space surface, $A_3 = \pi l^2$, as the union of both disks (see Fig. 3). The *surface* $A_{1\cup 3}(t)$ of two disks at center-to-center separation t is given by

$$A_{1\cup 3}(t) = \pi(l^2 - t^2) + 2l^2 \arcsin\left(\frac{t}{2l}\right) + \frac{t}{2}\sqrt{4l^2 - t^2}.$$

Note that a disk of radius t is blocked on account of the nearest-neighbor constraint resulting in $-\pi t^2$. Recall that the potential center positions of a nearest neighbor intersecting at $\boldsymbol{t}$ are homogeneously distributed on a disk of diameter l. For each t we choose this disk as the weighted disk representing the nearest neighbor. The effective diameter thus depends only on $|t|$:

$$c(|t|) := \frac{l_{\text{eff}}(|t|)}{l} = \left(\frac{A_{1\cup 3}(|t|)}{A_3}\right)^{1/2}. \quad (8)$$

Referring to Eq. (4), we account for the existence of segment 1 by resizing segment 3 to an effective length l_{eff} and make segment 3 the new segment 1. The newly formed segment is subjected to the same nearest-neighbor distribution as before; only the boundaries of the t integral change. The substitution $t' = tl$ reveals that c as defined in Eq. (8) has the desired effect:

$$P(r_{12}) = f^+(r_{12}) + [1 - f^+(r_{12})] \times \int_{-1/2}^{1/2} dt' l \int d\boldsymbol{r}_3 \omega^+(\boldsymbol{r}_3, lt') c(l|t'|) P(r_{32}). \quad (9)$$

Analogously to CPT, the percolation threshold is given by the smallest density that satisfies

$$0 = 1 - \int d\boldsymbol{r}_3 \int_{-1/2}^{1/2} dt' \omega^+(\boldsymbol{r}_3, lt') l_{\text{eff}}(l|t'|), \quad (10)$$

yielding $\rho_c l^2 \approx 5.83$, which is very close to the result of Monte Carlo simulations (cf. Table I). A good approximation of the mean cluster size can be computed as well (see Fig. 1). Detailed information is given in the Supplemental Material. For intermediate densities, the NNCPT prediction slightly deviates from the simulation results. Our choice of $c(|t|)$ is density independent and designed to yield a good approximation for the percolation threshold. However, the correct kernel $c(3, 2|3n1)$ depends on the density. A good approximation of $c(3, 2|3n1)$ at the percolation threshold is therefore expected to be less good for different densities. The divergence of the mean cluster size is characterized by the mean-field critical exponent $\gamma = 1$ if c does not depend on the density. This offers a different angle for interpreting critical exponents and outlines a way to improve on our closure. Usage of the nearest-neighbor distribution, however, provides the correct low density limit.

We can use the same closure to treat the percolation of ideal disks of area a and find $\rho_c a \approx 1.00$ which is also close to the simulation results [20]. The good agreement between NNCPT and simulation hinges on the fact that the nearest-neighbor construction describes loop structures in the cluster backbone implicitly, not explicitly as CPT. Moreover, NNCPT avoids an explicit density expansion by comprising all information on thermal correlations between particles in the nearest-neighbor distribution. This is particularly important if the critical density is as large as for ideal line segments. Furthermore, NNCPT bears the advantage that the kernel $c(3, 2|3n1)$ can be directly observed in simulations delineating a straightforward approach to assess the accuracy of the approximations made.

V. CONCLUSIONS

To summarize, we have introduced an alternative method to calculate continuum percolation thresholds. As two-dimensional systems are particularly challenging for standard methods of percolation theory, we have studied geometrical percolation of ideal line segments and disks in two dimensions and have shown that our method provides accurate predictions. The method can straightforwardly be applied to interacting and polydisperse systems in three dimensions as well. We therefore expect it to be of use in the design of composite materials.

ACKNOWLEDGMENTS

F.C. and T.S. acknowledge funding by the German Research Foundation in project 404913146. R.d.B. and P.v.d.S. acknowledge funding by the Institute for Complex Molecular Systems at Eindhoven University of Technology.

[1] H. Guo, N. Lin, Y. Chen, Z. Wang, Q. Xie, T. Zheng, N. Gao, S. Li, J. Kang, D. Cai, and D.-L. Peng, Sci. Rep. **3**, 2323 (2013).
[2] A. D. Pasquier, H. E. Unalan, A. Kanwal, S. Miller, and M. Chhowalla, Appl. Phys. Lett. **87**, 203511 (2005).
[3] I. Balberg, C. H. Anderson, S. Alexander, and N. Wagner, Phys. Rev. B **30**, 3933 (1984).
[4] S. Choi, S. I. Han, D. Kim, T. Hyeon, and D.-H. Kim, Chem. Soc. Rev. **48**, 1566 (2019).
[5] D. Jiang, V. Murugadoss, Y. Wang, J. Lin, T. Ding, Z. Wang, Q. Shao, C. Wang, H. Liu, N. Lu *et al.*, Polym. Rev. **59**, 280 (2019).
[6] Y. Huang, C. Ellingford, C. Bowen, T. McNally, D. Wu, and C. Wan, Int. Mater. Rev. **65**, 129 (2020).
[7] K. McLellan, Y. Yoon, S. N. Leung, and S. H. Ko, Adv. Mater. Technol. **5**, 1900939 (2020).
[8] C. Wang, J.-C. Chien, K. Takei, T. Takahashi, J. Nah, A. M. Niknejad, and A. Javey, Nano Lett. **12**, 1527 (2012).
[9] R. Valasma, E. Bozo, O. Pitkänen, T. Järvinen, A. Dombovari, M. Mohl, G. S. Lorite, J. Kiss, Z. Konya, and K. Kordas, Nanotechnology **31**, 305303 (2020).
[10] X. Cheng, Y. Gong, Y. Liu, Z. Wu, and X. Hu, Smart Mater. Struct. **29**, 075007 (2020).
[11] A. L. R. Bug, S. A. Safran, and I. Webman, Phys. Rev. Lett. **54**, 1412 (1985); Phys. Rev. B **33**, 4716 (1986).
[12] T. Schilling, M. A. Miller, and P. van der Schoot, Europhys. Lett. **111**, 56004 (2015).
[13] M.-A. Moradi, K. Larrakoetxea Angoitia, S. van Berkel, K. Gnanasekaran, H. Friedrich, J. P. Heuts, P. van der Schoot, and A. M. van Herk, Langmuir **31**, 11982 (2015).
[14] R. M. Mutiso and K. I. Winey, Phys. Rev. E **88**, 032134 (2013).
[15] R. F. Kayser and H. J. Raveché, Phys. Rev. A **17**, 2067 (1978).
[16] M. A. Bates and D. Frenkel, J. Chem. Phys. **112**, 10034 (2000).
[17] A. Coniglio, U. De Angelis, and A. Forlani, J. Phys. A: Math. Gen. **10**, 1123 (1977).
[18] J. P. Hansen and I. R. McDonald, *Theory of Simple Liquids: With Applications to Soft Matter*, 4th ed. (Elsevier, Oxford, 2013).
[19] T. Drwenski, S. Dussi, M. Dijkstra, R. van Roij, and P. van der Schoot, J. Chem. Phys. **147**, 224904 (2017).
[20] S. Mertens and C. Moore, Phys. Rev. E **86**, 061109 (2012).
[21] S. Torquato, *Random Heterogeneous Materials: Microstructure and Macroscopic Properties* (Springer, New York, 2002), Vol. 16.
[22] G. Tarjus, P. Viot, S. Ricci, and J. Talbot, Mol. Phys. **73**, 773 (1991).
[23] R. de Bruijn and P. van der Schoot (unpublished).
[24] S. Torquato, J. Chem. Phys. **136**, 054106 (2012).
[25] As shown by DeSimone and co-workers [27], this is already evident at the fourth virial level. While the two missing diagrams in the fourth hard-body virial cancel approximately, this is not the case for the fourth connectedness virial.
[26] G. Stell, J. Phys. A: Math. Gen. **17**, L855 (1984).
[27] T. DeSimone, S. Demoulini, and R. M. Stratt, J. Chem. Phys. **85**, 391 (1986).
[28] See Supplemental Material at http://link.aps.org/supplemental/10.1103/PhysRevE.103.042115 for a discussion on rotational invariant expansion and the cPY approximation. A more in-depth comparison of cPY approximation with Monte Carlo simulations are also included.
[29] J. D. Talman, J. Comput. Phys. **29**, 35 (1978).
[30] A. J. S. Hamilton, Mon. Not. R. Astron. Soc. **312**, 257 (2000).
[31] F. Coupette, A. Härtel, and T. Schilling, Phys. Rev. E **101**, 062126 (2020).